J Pharmacokinet Pharmacodyn (2014) 41:159–171
DOI 10.1007/s10928-014-9354-4

ORIGINAL PAPER

Physiologically based pharmacokinetic modelling of methotrexate and 6-mercaptopurine in adults and children. Part 1: methotrexate

Kayode Ogungbenro · Leon Aarons · The CRESim & Epi-CRESim Project Groups

Received: 15 November 2013 / Accepted: 6 March 2014 / Published online: 21 March 2014

Abstract Methotrexate is an antimetabolite and antifolate drug that is widely used in the treatment of malignancies and auto-immune disorders. In childhood acute lymphoblastic leukaemia, methotrexate is often combined with 6-mercaptopurine and both of them have been shown to be very effective for maintenance of remission. Large variability in the pharmacokinetics of methotrexate has led to increasing use of therapeutic drug monitoring in its clinical use to identify patients with high risk of toxicity and optimise clinical outcome. A physiologically based pharmacokinetic model was developed for methotrexate for oral and intravenous dosing and adults and paediatric use. The model has compartments for stomach, gut lumen, enterocyte, gut tissue, spleen, liver vascular, liver tissue, gall bladder, systemic plasma, red blood cells, kidney vascular, kidney tissue, skin, bone marrow, thymus, muscle and rest of body. A mechanistic model was also developed for the kidney to account for renal clearance of methotrexate via filtration and secretion. Variability on system and drug specific parameters was incorporated in the model to reflect observed clinical data and assuming the same pathways in adults and children, age-dependent changes in body size, organ volumes and plasma flows, the model was scaled to children. The model was developed successfully for adults and parameters such as net secretion clearance, biliary transit time and red blood cell distribution and binding parameters were estimated from published adult profiles. A relationship between fraction absorbed and dose using reported mean bioavailability data in the literature was also established. The model also incorporates non-linear binding in some tissues that has been described in the literature. Predictions using this model provide adequate description of observed plasma concentration data in adults and children. The model can be used to predict plasma and tissue concentrations of methotrexate following intravenous and oral dosing in adults and children and therefore help to improve clinical outcome.

Keywords Methotrexate · Pharmacokinetics · PBPK · Leukaemia · Arthritis · Modelling

Abbreviations

MTX	Methotrexate
6-MP	6-Mercaptopurine
ALL	Acute lymphoblastic leukaemia
PK	Pharmacokinetics
PBPK	Physiologically based pharmacokinetic
Cmax	Maximum concentration
RBC	Red blood cells
MTX-PG	Methotrexate polyglutamate
DHFR	Dihydofolate reductase
EHR	Enterohepatic recirculation
GFR	Glomerular filtration rate
BSA	Body surface area
BW	Body weight
HT	Height
CO	Cardiac output

K. Ogungbenro (✉) · L. Aarons
Centre for Applied Pharmacokinetic Research, Manchester Pharmacy School, The University of Manchester, Oxford Road, Manchester M13 9PT, UK
e-mail: kayode.ogungbenro@manchester.ac.uk

Introduction

Methotrexate (MTX) is an antimetabolite and antifolate drug that is widely used in the treatment of malignancies

such as acute lymphoblastic leukaemia (ALL) and autoimmune disorders such as arthritis, psoriasis and Crohn's disease [1]. Orally administered MTX has been shown to be very effective for maintenance of remission in childhood ALL [2]. The pharmacokinetics (PK) of MTX has been well described in the literature especially in adults. The volume of distribution is approximately equals to total body water [3, 4]. MTX is about 34 % bound to albumin in plasma [5]. Following intravenous dosing between 60 and 90 % of MTX is eliminated unchanged in urine, 10–30 % is eliminated through the bile and 1–9 % is metabolised by aldehyde oxidase into a 7-hydroxyl metabolite [4, 6, 7]. While glomerular filtration is the dominant pathway for renal elimination of MTX, both secretion and active reabsorption also play significant roles [4]. Orally administered MTX is rapidly and incompletely absorbed from the gut, and a dose dependent absorption process has been reported [4, 8]. Maximum plasma concentration (Cmax) is reached within 1.5 h of administration and the bioavailability of MTX is around 0.7 with a considerable variability [5]. It has also been reported that inside cells such as red blood cells (RBC), MTX undergoes polymerization to form methotrexate-polyglutamates (MTX-PG) which have been linked to its pharmacological activity [9–12].

MTX is associated with side-effects such as hepatotoxicity, nephrotoxicity, myelotoxicity, mucositis and neurological symptoms, some of which can be life threatening especially at high doses [13]. This combined with large variability in the PK of MTX has led to increasing use of therapeutic drug monitoring to identify patients with high risk of toxicity and optimal clinical outcome. Modelling and simulation has been widely used as a tool to understand variability, optimise dosage regimen and individualise dose in PK [14]. Population PK models based on two or three compartmental models have been developed for MTX, with the aim to optimise MTX dosing [15–20]. Physiologically based pharmacokinetic (PBPK) models have also been developed to explain the PK of MTX in human and animals. The PBPK model for MTX developed by Bischoff et al. [21, 22] represents one of the earliest attempts to predict tissue distribution of drugs in PK in different animal species and human. The model consists of 5 compartments for certain tissues and the model was not validated for orally administered MTX. Other attempts to build PBPK models for MTX have not overcome all of these problems [23–27]. The aim of the current work was to develop a PBPK model for MTX that is focused on children with ALL. The proposed model extended previously developed model to include key organs/tissues such as bone marrow, thymus and RBC. Since most of the parameters and data in the literature are available for adults, the plan was to develop a PBPK model in adults and then scaled to children. A PBPK model is ideal for scaling from adults to children because the model can be modified to reflect age-related changes in anatomical and physiological functions such as organ volumes, plasma flows and renal and enzymatic functions [28]. This work form part of child-rare-euro-simulation (CRESim) project which is an European union funded project designed to evaluate the role of modelling and simulation in the development of drugs for rare diseases. In this sub-project the disease is childhood ALL and the drugs that have been selected for the treatment are MTX and 6-MP, the PBPK models developed for these drugs will be combined with disease models developed under other work packages to obtain a model for clinical trial simulation.

Methodology

PBPK model development and assumptions

The PBPK model proposed for MTX in human comprises of the following compartments (Fig. 1a): stomach, gut lumen, enterocyte, gut tissue, spleen, liver vascular, liver tissue, gall bladder, systemic plasma, RBC, kidney vascular, kidney tissue, skin, bone marrow, thymus, muscle and rest of body. The rest of body compartment is used to account for mass balance of the system and the kidney and liver are considered the only sites of elimination [4, 6, 7]. Figure 1b shows a kidney model developed to account for renal clearance of MTX via filtration and secretion. This model in addition to compartments for kidney vascular and kidney tissue has compartments for glomerulus and proximal tubules. All tissues were modelled using well stirred assumption, unbound tissue concentration is at equilibrium with unbound concentration in the emergent plasma [29]. This can be described using

$$V_T \frac{dC_T}{dt} = Q_T \left(C_P - \frac{C_T}{K_{p,T}} \right) \quad (1)$$

where V_T, C_T, Q_T and $K_{p,T}$ represent the volume, concentration, plasma flow, tissue/plasma concentration ratio of the different tissues and C_P is the systemic plasma concentration.

It has been reported that MTX distribution in some tissues is non-linear especially at low concentrations, probably due to strong binding of MTX to dihydrofolate reductase (DHFR) in these tissues [22, 30]. Tissue concentrations are therefore modelled as the sum of linear non-specific binding and strong binding that is associated with DHFR and is given by

$$C_T = R_T \cdot C_P + \frac{a_T \cdot C_P}{\varepsilon_T + C_P} \quad (2)$$

$$K_{p,T} = \frac{C_T}{C_P} = R_T + \frac{a_T}{\varepsilon_T + C_P} \quad (3)$$

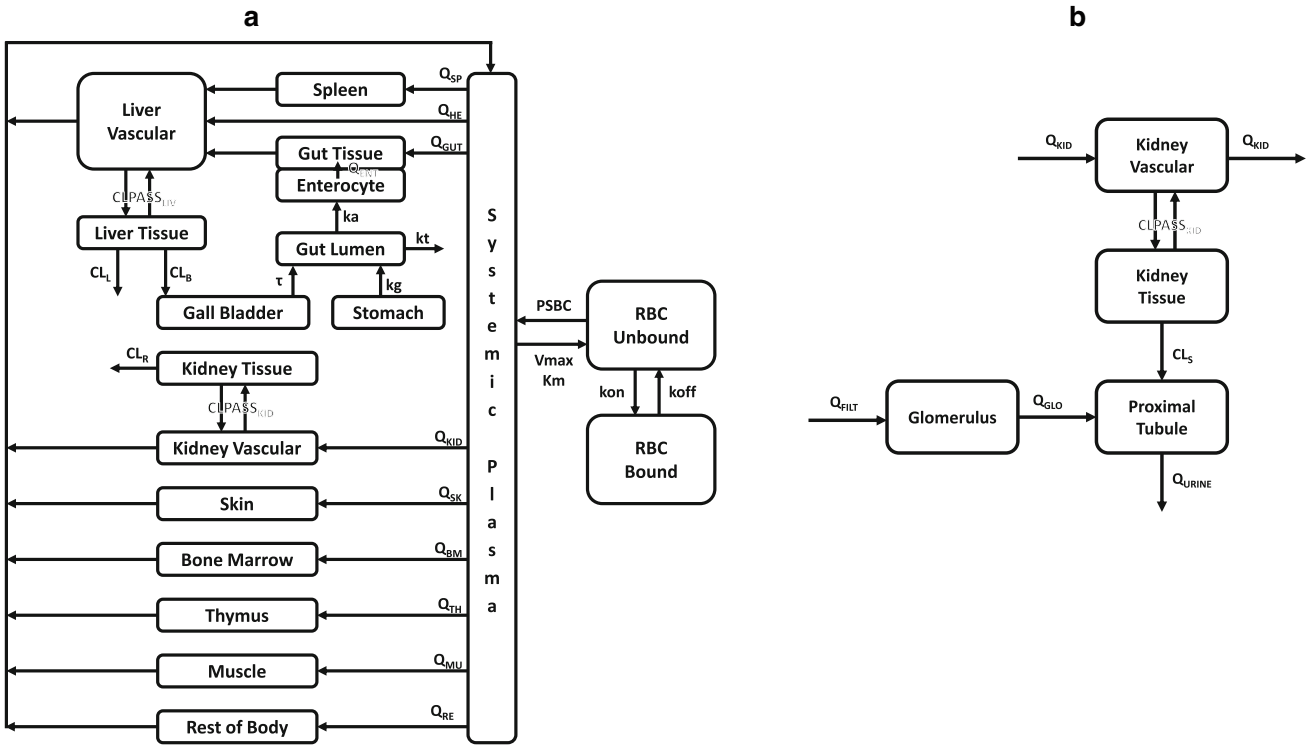

Fig. 1 **a** Physiologically based pharmacokinetic model describing the kinetics of methotrexate **b** kidney model describing the renal clearance of methotrexate

where R_T, a_T and ε_T are linear binding, strong specific binding and DHFR dissociation terms respectively [22, 30].

Enterohepatic recirculation (EHR) was modelled using a transit compartment that allows a time delay for emptying of the bile into the gut lumen. The biliary secretion and transit were modelled as follows

$$\frac{dr}{dt} = \left(\frac{CL_B \cdot fu \cdot C_{LIV,T}}{K_{p,LIV}} - r\right) \Big/ \tau \tag{4}$$

where r, fu, $C_{LIV,T}$, CL_B, $K_{p,LIV}$ and τ are the biliary secretion parameter, fraction unbound in plasma, liver tissue concentration, biliary clearance, liver/plasma concentration ratio and transit time respectively.

Liver and kidney tissues were separated into vascular and tissue compartments with passive clearances between the two compartments set to 10,000 times the plasma flows to these tissues. This allows the flow limited assumption to be preserved for these tissues. The volumes of the vascular compartments were set to 10 % of the volumes of the organs.

Intracellular RBC MTX concentration was modelled assuming saturable uptake of unbound plasma MTX concentration into RBC and a passive efflux from RBC. It was assumed that inside RBC, MTX binds to intracellular proteins, a process described using *kon* and *koff* parameters. Total MTX-PG intracellular RBC concentration was modelled although it is possible to modify the model to reflect individual MTX-PG [12, 31].

Hepatic (CL_L) and biliary (CL_B) intrinsic clearance parameters were back calculated from reported in vivo estimates assuming well stirred model. Stewart et al. [32] reported systemic clearance for MTX following intravenous dosing and the renal component of the total clearance was also reported. The contribution of the biliary route to the total systemic in vivo clearance has also been reported for different studies [7, 33]. Renal clearance was separated into filtration and net secretion. The filtration component (Q_{FILT}) was obtained as a function of glomerular filtration rate (GFR) using

$$Q_{FILT} = fu \cdot GFR \cdot C_P \tag{5}$$

while the net secretion component (CL_S) was obtained from fitting the PBPK model to some clinical data.

A first-order process was assumed for oral absorption of MTX from the gut lumen and it was assumed that there is no metabolism in the gut. However, due to the reported non-linear relationship between dose and bioavailability [8], it was assumed in the model that the non-linearity is due to fraction absorbed (F_a), such that both intestinal availability (F_G) and hepatic availability (F_H) were assumed to be 1. To establish a relationship between F_a and dose, data from clinical studies were obtained from the literature on reported mean absolute bioavailability. An initial attempt by Teresi

Table 1 Organ/tissue volumes (V) and plasma flows (Q) for adults and binding parameters (R = linear binding, a = non-linear binding and ε = dissociation constants) for different tissues/organs in the PBPK

Parameters	Organs/tissues										
	Plasma	Muscle	Kidney	Liver	Gut	Enterocyte	Skin	Bone marrow	Spleen	Thymus	Rest of body
V (L)[a]	2.9	29	0.3	1.8	1.7	0.1	3.3	1.2	0.15	0.025	–[§§]
Q (L/h)[a]	196[§]	36.5	43.7	14	30	11.8	10.7	5.9	6.4	2.9	–[§§§]
R[b]	–	0.15	3	3	1	–	1	1	1	1	0.15
a (mg/L)[b]	–	–	0.3	0.4	0.1	–	–	0.2	0.1	0.1	–
ε (mg/L)[b]	–	–	0.00001	0.00001	0.00001	–	–	0.00001	0.00001	0.00001	–

[a] Obtained from references [34] and [35]

[b] Obtained from references [22] and [30]

[§] cardiac output, $§§ = 70 - \sum_T V_T$, $§§§ = 196 - \sum_T Q_T$

et al. [8] to establish a relationship between oral bioavailability and dose resulted in two values for doses greater than or less than 40 mg/m^2. More data were added to the data used in Teresi et al. [8] so that a continuous relationship can be established between F_a and dose.

System and drug specific parameters

The relevant system and drug-specific parameters for adults (18–20 years old, body weight 70 kg) were obtained from the literature. Organ/tissue volumes and plasma flows are presented in Table 1 [34, 35]. Parameters for the linear and strong non-linear binding to DHFR are also presented in Table 1 [22, 30]. Other system and drug specific parameters used in the PBPK model are presented in Tables 2 and 3 respectively. The 'rest of body' was assumed to have the same parameter tissue/plasma partition coefficient as the muscle. Parameters for distribution of MTX into the RBC were estimated by fitting the PBPK model to reported plasma and RBC concentrations. Other parameters estimated were CL_S and τ. Parameter estimation was performed using mean plasma data from four different studies following a single intravenous dose of MTX at 15 mg (Stewart et al. [32], Seideman et al. [6]), 50 mg (Schornagel et al. [36]) and 100 mg/m^2 (Stewart et al. [37]) and total RBC MTX-PG concentration from one study following oral dosing of 10 mg/week for 36 weeks and 20 mg/week for 88 weeks respectively in two patients. The model was fitted using *lsqnonlin* function in MATLAB and the percentage relative standard errors, SE% were obtained using the equation described by Landaw et al. [38].

Scaling

Scaling of the developed PBPK model from adults to children was based on the assumption that elimination pathways in adults and children are the same. Age-dependent changes in body size, organ volumes and plasma flows were used to scale the PBPK model. Cardiac output (CO) was predicted for children using the equation derived in Johnson et al. [39]. Reference values for body weight (BW) and height (HT) were obtained from the literature [34], and BSA was predicted using Haycock and Dubois equations [40, 41]. Reference values for organ/tissue flows and volumes were obtained for 0, 1, 5 10 and 15 year old for the different organs/tissues in the PBPK model [34, 35]. These reference organ/tissue volumes and plasma flows were expressed as the fraction of BW and CO for the different ages. For ages in between, a simple linear interpolation was used to obtain fractions of organ/tissue volumes and plasma flows. It is therefore possible to simulate organ/tissue volumes and plasma flows from these fractions for any paediatric age by simulating the BW, HT and CO. Reference values for total blood volume and haematocrit

Table 2 Other system parameters used in the PBPK model for adults

Parameter	Definition	Value	Source
kg (h^{-1})	Stomach emptying rate constant	2	[34]
kt (h^{-1})	Intestinal transit rate constant	0.25	[34]
Q_{ENT} (L/h)	Enterocytic plasma flow	11.76	[29, 58]
V_{ENT} (L)	Volume of enterocyte	0.12	[29]
Q_{GLO} (L/h)	Glomerular flow rate	7.5	[59]
Q_{URINE} (L/h)	Flow rate into the loop of Helen	2.7	[59]
V_{GLO} (L)	Volume of Glomerulus	0.03	[34]
V_{PROX} (L)	Volume of proximal tubule	0.094	[34, 35]
BSA (m^2)	Body surface area	1.85	[34]
HT (m)	Height	1.76	[34]
BW (kg)	Body weight	70	[34]
GFR (L/h)	Glomerular flow rate	13.5	[39]
alb (g/L)	Plasma albumin level	37.0	[39]
V_{RBC} (L)	Volume of RBC	2.4	[34]
HCT	Haematocrit	0.45	[34]

Table 3 Other drug-specific parameters used in the PBPK model for adults

Parameter	Definition	Value	Source
MW (g)	Molecular weight	454.4	–
fu	Plasma fraction unbound	0.68	[5, 60]
ka (h^{-1})	Absorption rate constant	2.8	[49]
CL_L (L/h)	Intrinsic hepatic clearance	0.18	[7, 33]
CL_B (L/h)	Intrinsic biliary clearance	3.3	[7, 33]
CL_S (L/h)	Net renal secretion clearance	13.5 (4.6)[a]	–[b]
PSBC (L/h)	RBC permeability surface area product	0.741 (2.6)	–[b]
Vmax (mg/L h)	RBC maximum uptake rate	0.0034 (5.1)	–[b]
Km (mg/L)	RBC uptake Michaelis constant	0.0005 (5.2)	–[b]
kon (h^{-1})	RBC association constant	0.0323 (46.8)	–[b]
koff (h^{-1})	RBC dissociation constant	0.0007 (4.6)	–[b]
τ (h)	Biliary transit time	7.7 (28.3)	–[b]

[a] SE (%)

[b] Estimated

for different paediatric age groups were also obtained from the literature [34, 42]. RBC distribution and binding parameters were assumed to be the same in adults and children. Mean glomerular filtration rate (GFR) for the different paediatric age groups was obtained from the data published in Johnson et al. [39]. Plasma protein binding was estimated for children using the equations presented by McNamara and Alcorn [43]. Reference values for albumin for different paediatric age groups was obtained using the equation presented in Johnson et al. [39]. In children, both CL_L and CL_B were scaled by allometry [44]

$$CL_{L,paed} = CL_{L,ad} \cdot \left(\frac{BW_{paed}}{BW_{ad}}\right)^{0.75} \quad (6)$$

$$CL_{B,paed} = CL_{B,ad} \cdot \left(\frac{BW_{paed}}{BW_{ad}}\right)^{0.75} \quad (7)$$

where $CL_{L,paed}$, $CL_{L,ad}$, $CL_{B,paed}$, $CL_{B,ad}$, BW_{paed} and BW_{ad} are metabolic clearance in children, metabolic clearance in adults, biliary clearance in children, biliary clearance in adults, BW in children and BW in adults respectively.

Variability

Variability was introduced on the parameters of the PBPK model so that the simulated profiles using the PBPK model were comparable with observed data in different age groups. The main sources of variability in the PBPK model were BW and BSA. Variability on BW propagates through organ volumes and variability on BSA propagates through CO and therefore through organ/tissue plasma flows. Variabilities were also introduced on other system parameters such as *GFR*, *kg* (stomach emptying rate), and *kt* (intestinal transit rate) and drug-specific parameters such as *R*, CL_L, CL_B, CL_S, *PSBC*, *Vmax*, *Km*, *kon*, *koff*, *ka* and τ. Parameters were simulated assuming lognormal distribution with a coefficient of variation (CV) of 20 %.

Simulation

To evaluate the performance of the developed PBPK model, the literature was searched for studies that reported plasma concentrations following intravenous and oral dosing of MTX in adults or children. In some cases plasma concentration–time profiles for individuals were reported and in others cases mean profiles with standard deviation (SD) or standard error (SE) bars for each time points were reported. Data from graphs were digitized using GetData Graph Digitizer [45]. Simulations using the PBPK model were made to match the reported mean age of published clinical data, adult studies were assumed to be for adults and simulated parameters were made to reflect this. Most anti-cancer drugs including MTX are often dosed based on BSA [46] and in most cases the BSA were not reported, in these cases reference BSA were computed based on the mean age of the patients. A virtual population of 1,000 individuals was simulated in all cases and these were used to compute the 2.5, 50 and 97.5th percentiles. The simulated plasma concentration–time curves were superimposed on the observed individual data points or the mean profiles with SD bars.

Results

The differential equations ("Appendix") that describe the concentration in various tissues/organs of the PBPK model (Fig. 1a) were implemented in MATLAB software [47], this was also used for all simulations. The data obtained for bioavailability from different studies in the literature and used to estimate F_a is presented in Fig. 2. The figure shows mean F_a (obtained from mean bioavailability) plotted against mean dose (mg/m^2 of BSA). The data was obtained from 18 published studies. An Emax model was fitted to the data to describe the nonlinear relationship between F_a and dose, using

$$F_a = 1 - Emax \cdot dose/(ED50 + dose) \quad (8)$$

The model was fitted using *lsqnonlin* function in MATLAB and the parameter estimates (*SE* %) were 0.77 (6.0 %) and 15.01 (31.4 %) for *Emax* and *ED*50 respectively

The parameter estimates obtained from fitting plasma concentration data and RBC MTX-PG data are shown in Table 3 and the fitted plasma profiles with the data are shown in Fig. 3. The parameters were estimated with good precision as reflected by the *SE* %.

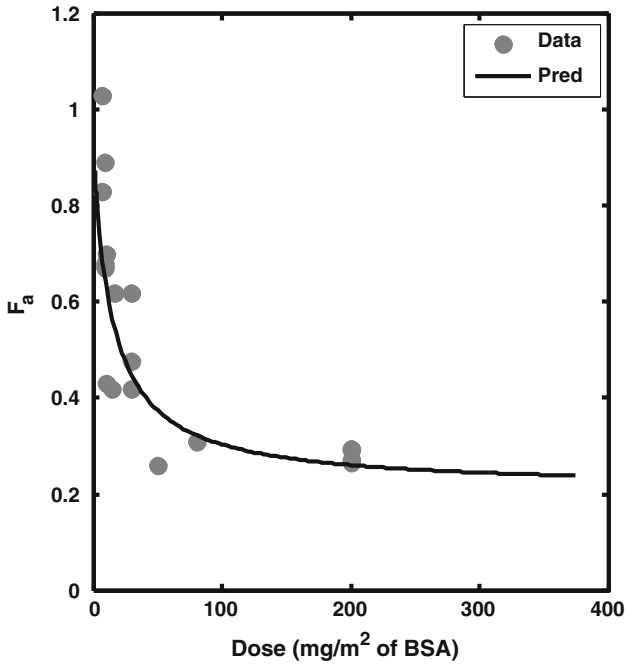

Fig. 2 Relationship between fraction absorbed (F_a) and oral dose of methotrexate

Simulated mean tissue concentration–time profiles for MTX in plasma, muscle, kidney, liver, gut, bone marrow, thymus and RBC in 5, 10 and 18 year old subjects following 25 mg oral dosing are shown in Fig. 4. The profiles in plasma and tissues appear to fall in two phase; a rapid decline of the profiles is followed by a slower decline. For tissues such as kidney, liver, gut, bone marrow and thymus the second phase is slower than what has been observed in plasma and muscle, the plateau observed in this terminal phase is probably due to strong binding of MTX to DHFR. This type of pattern has been demonstrated in a number of studies in rats and in some of these tissues, the observed MTX plateau concentration has been linked to the concentration of DHFR [25, 30].

Observed plasma concentration data for MTX following intravenous dosing in adults from three different studies are presented in Fig. 5 and superimposed on these are the simulated 2.5, 50 and 97.5th percentiles. The data in Fig. 5a was obtained from 12 rheumatoid arthritis patients who received 15 mg of MTX as a bolus dose [48]. The data was digitized from individual profiles. The data in Fig. 5b was obtained from 37 patients with advanced head and neck cancer who received 100 mg/m^2 of MTX as an intravenous bolus dose [37]. The data in the original publication was plotted as median and interquartile range at different time points after dosing. The data in Fig. 5c was obtained from 10 rheumatoid arthritis patients who received 15 mg MTX as an intravenous bolus dose [49]. Individual MTX plasma concentration–time profiles plotted in the publication were digitized. Observed plasma concentration data, superimposed with simulated profiles

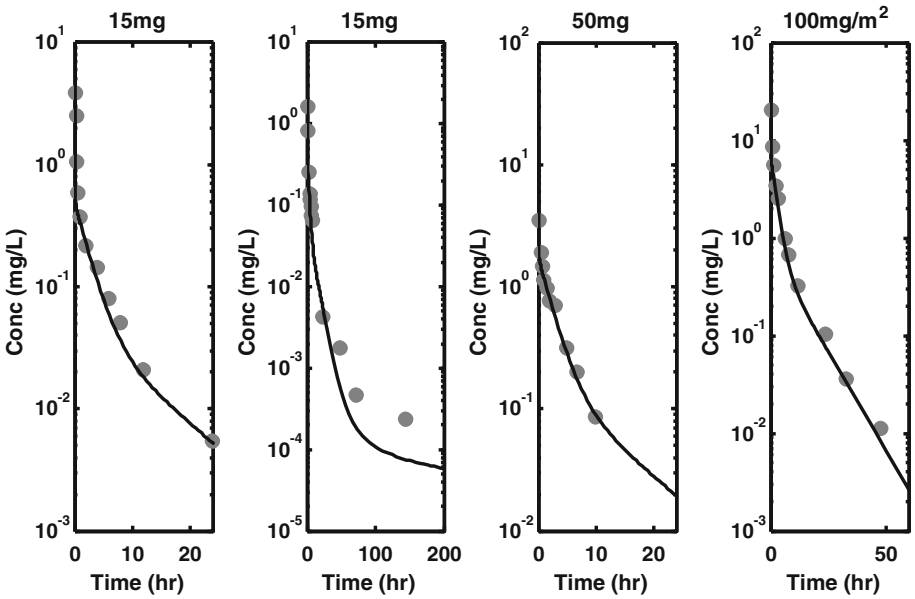

Fig. 3 Fitted PBPK model profile and mean observed plasma concentration data from four different studies following a single intravenous dose of MTX at 15 mg (Stewart et al. [32], Seideman et al. [6]), 50 mg (Schornagel et al. [36]) and 100 mg/m^2 (Stewart et al. [37])

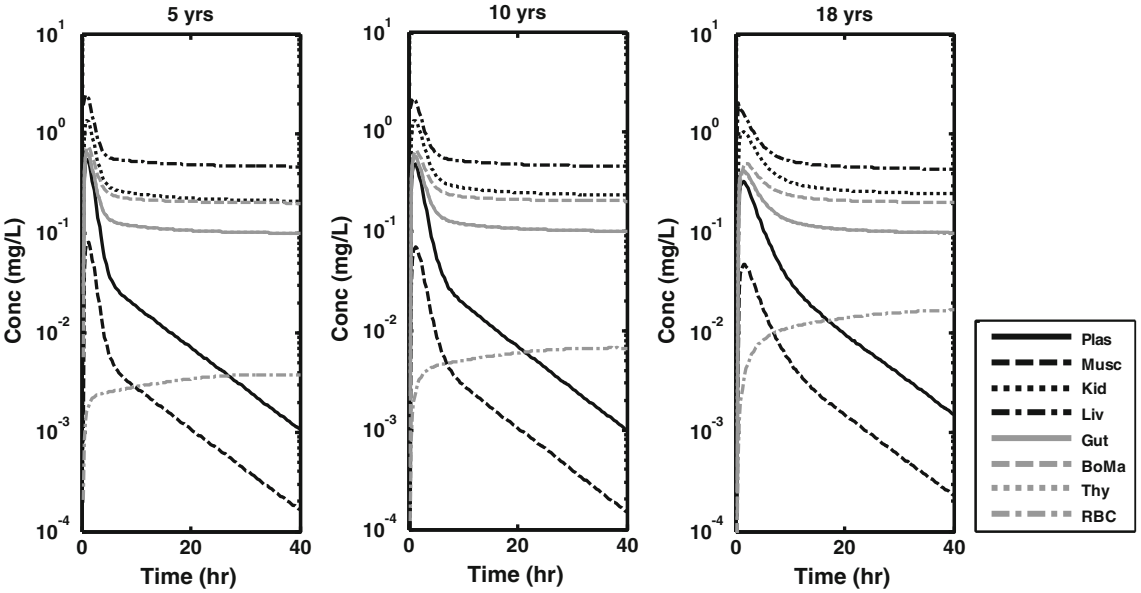

Fig. 4 Simulated mean concentration–time profiles of methotrexate in plasma (Plas), muscle (Musc), kidney (Kid), liver (Liv), gut (Gut), bone marrow (BoMa), thymus (Thy) and red blood cells (RBC) following oral dosing of 25 mg to 5, 10 and 18 years old subjects

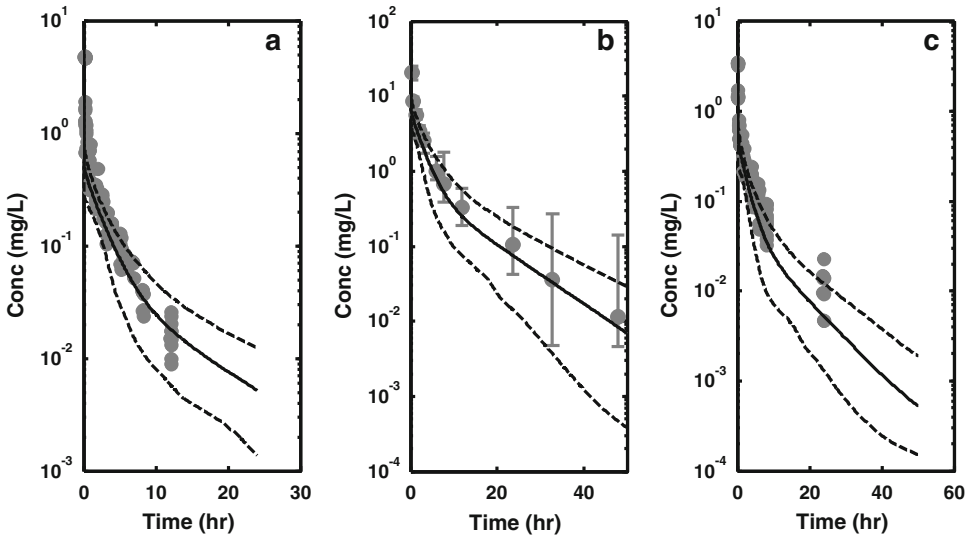

Fig. 5 Observed and predicted plasma concentration–time profiles (2.5, 50 and 97.5th percentiles) of methotrexate following intravenous dosing in three different studies in adults **a** 15 mg (Hubner et al. [48]), **b** 100 mg/m^2 (Stewart et al. [37]), **c** 15 mg (Oguey et al. [49])

following oral dosing of MTX in adults from three different studies are presented in Fig. 6. The data in Fig. 6a was obtained from 12 rheumatoid arthritis patients who received a 15 mg dose of MTX [32]. The data was plotted as mean and standard deviation bars at different time points in the publication. The data in Fig. 6b was obtained from 16 psoriatic patients who received a 10 mg dose of MTX orally. The data in Fig. 6c was obtained from 12 healthy men who received a 7.5 mg dose of MTX orally with and without food. Individual data were not provided but the mean profiles from the two occasions were plotted and these were digitized.

Observed plasma concentration data from studies in children were also superimposed with simulated profiles obtained using the information provided in the original studies. Figure 7a, b and c were from studies where MTX has been given intravenously. The data in Fig. 7a was obtained from a study where 15 mg/m^2 of MTX was administered to ALL children as an intravenous bolus dose [50]. Plasma concentrations were collected at 12 time points and between 5 and 18 patients were sampled at each time point. Mean plasma concentration and standard error of the mean were reported for each time point. The mean age of children in the study was 9.5 year (range 3–16 year)

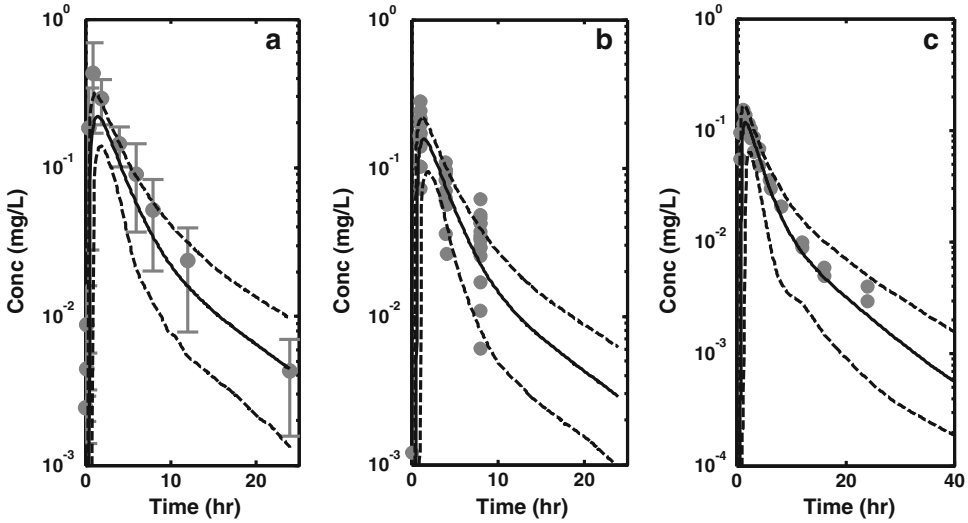

Fig. 6 Observed and predicted plasma concentration–time profiles (2.5, 50 and 97.5th percentiles) of methotrexate following oral dosing in three different studies in adults **a** 15 mg (Stewart et al. [32]), **b** 10 mg (Hroch et al. [61]), **c** 7.5 mg (Kozloski et al. [62])

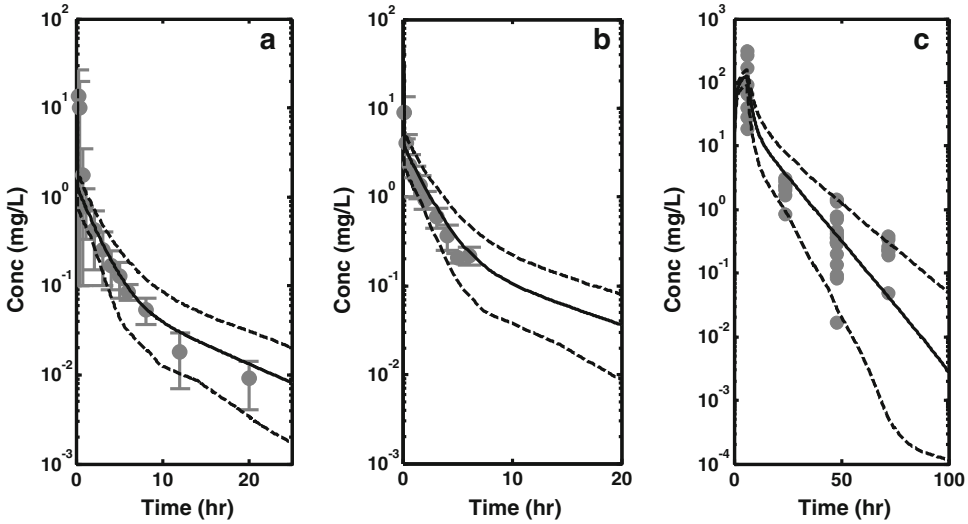

Fig. 7 Observed and predicted plasma concentration–time profiles (2.5, 50 and 97.5th percentiles) of methotrexate following intravenous dosing in three different studies in children **a** 15 mg/m^2 (Pinkerton et al. [50]), **b** 40 mg/m^2 (Teresi et al. [8]), **c** 150 mg/kg (Wang et al. [51])

therefore the simulated profiles plotted in Fig. 7a are for a 9.5 year old child. The data in Fig. 7b was obtained from a study where 40 mg/m^2 of MTX was administered to ALL children as an intravenous bolus dose [8]. Plasma concentrations were collected at 7 time points after dosing from 12 patients. Mean plasma concentration and standard deviation bars were plotted against time in the original publication. The mean age of children in the study was 5.5 year (range 1.9–18.1 year), the simulated profiles plotted in Fig. 7b are therefore for a 5.5 year old child. The data in Fig. 7c was obtained from a study where 150 mg/kg of MTX was administered to children with osteosarcoma as a 6 h intravenous infusion [51]. Plasma concentrations were collected at 4 time points after dosing from 52 patients. Individual plasma concentrations were plotted against time in the original publication. The data plotted in Fig. 7c is for less than 10 year old children in the study and the simulated profiles plotted in Fig. 7c are for a 5 year old child.

The data in Fig. 8a was obtained from a study where 15 mg/m^2 of MTX was administered to ALL children orally [50]. Plasma concentrations were collected at 12 time points and between 5 and 23 patients were sampled at each time point. Mean plasma concentration and standard error of the mean were reported for each time point in the original publication. The mean age of children in the study was 9.5 year (range 3–16 year) and the simulated profiles plotted in Fig. 8a are for a 9.5 year old child. The data in Fig. 8b was obtained from a single ALL patient who was on maintenance dose of MTX at 4 different cycles [52]. Plasma concentration was obtained at 7 time points per cycle and this was plotted against time. The simulated profiles plotted in Fig. 8b are for a 4.5 year old child who received a 18 mg/m^2 dose of MTX. The data in Fig. 8c was

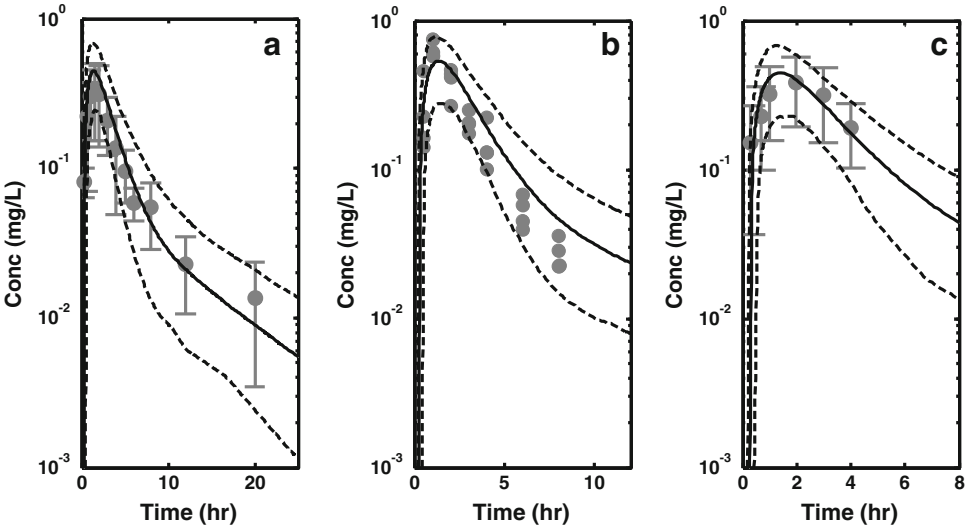

Fig. 8 Observed and predicted plasma concentration–time profiles (2.5, 50 and 97.5th percentiles) of methotrexate following oral dosing in three different studies in children **a** 15 mg/m^2 (Pinkerton et al. [50]), **b** 18 mg/m^2 (Balis et al. [52]), **c** 15 mg/m^2 (Pinkerton et al. [53])

obtained from a study where 15 mg/m^2 of MTX was administered to ALL children orally [53]. Plasma concentrations were collected at 6 time points in 20 subjects. Mean plasma concentration and standard deviation bars were plotted against time in the original publication. The children in the study were between 3 and 16 year old and the simulated profiles plotted in Fig. 8c are for a 9.5 year old child.

Discussion and conclusion

In this study a PBPK model has been developed for prediction of plasma and tissue concentrations of MTX in adults and children following intravenous and oral dosing. The approach that has been used was to develop and validate a PBPK model first in adults and then scale this to children using age-dependent anatomical and physiological information available in the literature. This is similar to a workflow recently published for developing a PBPK model to support paediatric research and development using Lorazepam as a case study [54].

The PBPK model developed in this study has separate compartments for key organs/tissues and specific issues that have been raised in the literature on the absorption, distribution, metabolism and excretion of MTX were also accounted for in the model. MTX absorption is very complex; it has been described as rapid, incomplete and variable [4]. It has been reported that absorption follows first or zero order kinetics depending on the patient, and in the current study first order kinetics was assumed. Also the absorption rate constant was assumed to be the same for adults and children based on available in vivo clinical data. In a study that involved 28 ALL patients aged 3–16 years, 15 mg/m^2 of MTX was administered intravenously and/or orally [50]. It was reported that there was no correlation between rate of absorption and patient's age, sex, duration of therapy or treatment schedule.

The bioavailability of MTX has been reported to be dose dependent and this was incorporated as a function of F_a in the PBPK model described in the present work. The trend of decreasing bioavailability with increasing doses has been reported in adults and children [8]. Data collected from the literature was used to establish a non-linear relationship between F_a and dose. In a clinical study in 12 ALL patients, bioavailability was determined by comparing the area under the concentration–time profile after intravenous and oral doses between 13 and 76 mg/m^2 [8]. The mean bioavailability for doses $\leq$40 (13–40) mg/m^2 was 0.42 (0.19–0.76) and for doses $\geq$40 (43–76) mg/m^2 bioavailability was 0.18 (0.13–0.22). Based on the non-linear relationship between F_a and dose established in the current work for 30 and 60 mg/m^2 the values of F_a were 0.44 and 0.35.

The model developed for MTX in the current study also incorporated different routes of elimination of MTX that have been studied in the literature. Renal elimination is the most significant route of elimination and therefore a kidney model that separates filtration from net secretion was developed. This work represents the first time such a model has been implemented for MTX. Apart from filtration active renal secretion and active reabsorption have both been reported to be involved in the elimination of MTX and it has been reported that both routes are saturable at different concentrations. Due to lack of data it is impossible to separate active renal secretion from reabsorption in the present work and therefore a simple net secretion clearance parameter, CL_S was incorporated in the model. This parameter together with other drug specific parameters was estimated using published plasma-concentration

time profile data. Johansson et al. [18] implemented a similar approach in a population pharmacokinetic/pharmacodynamic model developed for MTX plasma concentration and mucositis scores in osteosarcoma patients. In the model clearance was separated into filtration as a function of GFR and secretion/metabolism; an estimate for the latter was obtained from the fitting. The estimate obtained for the fixed effect parameter of the secretion/metabolism component was 10.9 L/h and in the present work the estimate for CL_S was 13.5 L/h, assuming a well stirred model this gave plasma clearance estimate of 7.6 L/h. Liver and kidney tissues were separated into vascular and tissue compartments, this is not expected to have any advantage over single compartments for these tissues but it will allow future development of the model to incorporate transporter effects. MTX has been reported to be a substrate for a number of transporters such as OAT1, BCRP, MRP2, OATP1B1 etc. in the kidney and liver [55–57]. Parameter estimates for these transporters can be incorporated into this model both in the kidney and liver to reflect uptake and efflux mechanisms.

A simple transit compartment was implemented in the model to account for EHR of MTX. It is difficult to assess the contribution of EHR to the PK profiles of MTX especially since secondary peaks are not obvious following intravenous or oral dosing. However it has been reported that EHR play a significant role in the PK of MTX. Breithaupt et al. [7] provided one of the most compelling evidence for biliary excretion and EHR of MTX in humans. Firstly they noticed a considerable amount of MTX in the gastric juice vomited by osteosarcoma patients at the end of high dose intravenous MTX infusion. Also they noticed that plasma concentration–time profiles of MTX following intravenous infusion was influenced by coadministration of oral activated charcoal. In the study, 5 and 10 g activated charcoal were given daily for 3 days beginning 12 h before the start of the high dose intravenous MTX infusion. It was reported that plasma concentration–time profiles of high dose intravenous MTX infusion during co-administration with activated charcoal was lower compared with the control. The difference between the plasma concentration–time profiles of MTX during coadministration with 10 g activated charcoal and control was about 30 %.

The simulated MTX concentration profile in RBC shows that uptake of MTX is a very slow process and therefore equilibrium with plasma take a long time to establish and the profile continues to rise for a long time after dosing. This may be due to the activity of the transporters responsible for transportation of MTX into these cells. The profiles in the tissues (especially in plasma) decline fastest in 5 year old followed by 10 years old. This is possibly due to the changes in elimination as a function of age. The data used to estimate the parameters that describe the concentration of intracellular RBC MTX-PG was obtained from representative individuals reported in a clinical study. It is therefore important that this part of the model is validated and improved if necessary using a larger dataset. Also total MTX-PG has been considered in the model but it is possible to extend this part of the model to incorporate individual MTX-PG. A population PK model was published recently for MTX and its polyglutamated metabolites in RBC, and the approach used in this publication could be used to further improve this work to described individual MTX-PG in RBC. Although it has been suggested that MTX-PG can be useful for monitoring MTX in rheumatoid arthritis, the exact correlation between MTX-PG and efficacy is still not yet established [12].

The simulated profiles using the developed PBPK model showed acceptable coverage of the observed data obtained from the literature for adults and children following intravenous and oral dosing in all cases. In adults there is slight under-prediction of the initial concentrations especially immediately after intravenous dosing. This may be due to the assumption that the adults were 18 year old and therefore the simulations were based on physiological parameters for this age whereas some of the studies included patients/volunteers that are older.

In conclusion, a PBPK model that describes the PK of MTX in humans has been developed and this model can be used to predict plasma and tissue concentrations in both adults and children following intravenous and oral administration. The model incorporates various particular issues that have been raised in the literature on the PK of MTX and predictions using this model with variability on system and drug specific parameters provide adequate description of the observed plasma concentration data in adults and children.

Acknowledgments This work performed as part of Child-Rare-Euro-Simulation Project. CRESim was funded by the ERA-NET PRIOMEDCHILD Joint Call in 2010. Members of the CRESim Project Group: Leon Aarons; Agathe Bajard; Clément Ballot; Yves Bertrand; Frank Bretz; Daan Caudri; Charlotte Castellan; Sylvie Chabaud; Catherine Cornu; Frank Dufour; Nathalie Eymard; Roland Fisch; Renzo Guerrini; Vincent Jullien; Behrouz Kassaï; Patrice Nony; Kayode Ogungbenro; David Pérol; Gérard Pons; Harm Tiddens; Anna Rosati. Members of the Epi-CRESim Project Group: Corinne Alberti; Catherine Chiron; Catherine Cornu, Polina Kurbatova; Rima Nabbout. The authors also acknowledge helpful discussions with Dr Aleksandra Galetin, Dr Michael Gertz, Dr Eleanor Howgate, Dr Henry Pertinez, Nikolaos Tsamandouras, Adam Darwich and members of the Centre for Applied Pharmacokinetic Research, Manchester Pharmacy School.

Appendix

Equations that describe the concentration in different tissues/organs of the PBPK model for methotrexate

(1) Systemic Plasma

$$V_P\frac{dC_P}{dt} = (Q_{HE}+Q_{GUT}+Q_{ENT}+Q_{SP})C_{LIV,V} + Q_{KID}C_{KID,V} + \frac{Q_{MU}C_{MU}}{K_{p,MU}} + \frac{Q_{SK}C_{SK}}{K_{p,SK}} + \frac{Q_{BM}C_{BM}}{K_{p,BM}} + \frac{Q_{TH}C_{TH}}{K_{p,TH}} + \frac{Q_{RE}C_{RE}}{K_{p,RE}} + Q_{HE} + Q_{GUT} + Q_{ENT} + Q_{KID} + Q_{MU} + Q_{SK} + Q_{SP} + Q_{BM} + Q_{TH} + Q_{RE})C_P - \left(\frac{V\text{maxfuC}_\text{P}}{Km+fuC_P}\right)V_P + PSBCC_{RBC,U}$$

(2) Muscle

$$V_{MU}\frac{dC_{MU}}{dt} = Q_{MU}\left(C_P - \frac{C_{MU}}{K_{p,MU}}\right)$$

(3) Kidney Vascular

$$V_{KID,V}\frac{dC_{KID,V}}{dt} = Q_{KID}\left(C_P - C_{KID,V}\right) - CLPASS_{KID}fuC_{KID,V} + \frac{CLPASS_{KID}fuC_{KID,T}}{K_{p,KID}}$$

Tissue

$$V_{KID,T}\frac{dC_{KID,T}}{dt} = CLPASS_{KID}fuC_{KID,V} - \frac{CLPASS_{KID}fuC_{KID,T}}{K_{p,KID}} - \frac{CL_SfuC_{KID,T}}{K_{p,KID}}$$

Glomerulus

$$V_{GLO}\frac{dC_{GLO}}{dt} = GFRfuC_P - Q_{GLO}C_{GLO}$$

Proximal Tubule

$$V_{PROX}\frac{dC_{PROX}}{dt} = Q_{GLO}C_{GLO} + \frac{CL_sfuC_{KID,T}}{K_{p,KID}} - Q_{URINE}C_{PROX}$$

(4) Liver

Vascular

$$V_{LIV,V}\frac{dC_{LIV,V}}{dt} = Q_{HE}\left(C_P - C_{LIV,V}\right) - CLPASS_{LIV}fuC_{LIV,V} + \frac{CLPASS_{LIV}fuC_{LIV,T}}{K_{p,LIV}} + \frac{(Q_{GUT}+Q_{ENT})C_{GUT}}{K_{p,GUT}} - (Q_{GUT}+Q_{ENT})C_{LIV,V} + \frac{Q_{SP}C_{SP}}{K_{p,SP}} - Q_{SP}C_{LIV,V} + Q_{ENT}C_{ENT}$$

Tissue

$$V_{LIV,T}\frac{dC_{LIV,T}}{dt} = CLPASS_{LIV}fuC_{LIV,V} - \frac{CLPASS_{LIV}fuC_{LIV,T}}{K_{p,LIV}} - \frac{(CL_L+CL_B)fuC_{LIV,T}}{K_{p,LIV}}$$

(5) Gut

Tissue

$$V_{GUT}\frac{dC_{GUT}}{dt} = (Q_{GUT}+Q_{ENT})\left(C_P - \frac{C_{GUT}}{K_{p,GUT}}\right)$$

Lumen

$$\frac{dA_{LUM}}{dt} = kgA_{ST} - kaA_{LUM} - ktA_{LUM} + r$$

Enterocyte

$$V_{ENT}\frac{dC_{ENT}}{dt} = kaA_{LUM} - Q_{ENT}C_{ENT}$$

(6) Stomach

$$\frac{dA_{ST}}{dt} = -kgA_{ST}$$

(7) Biliary Transit

$$\frac{dr}{dt} = \left(\frac{CL_BfuC_{LIV,T}}{K_{p,LIV}} - r\right)\Big/\tau$$

(8) Skin

$$V_{SK}\frac{dC_{SK}}{dt} = Q_{SK}\left(C_P - \frac{C_{SK}}{K_{p,SK}}\right)$$

(9) Bone Marrow

$$V_{BM}\frac{dC_{BM}}{dt} = Q_{BM}\left(C_P - \frac{C_{BM}}{K_{p,BM}}\right)$$

(10) Spleen

$$V_{SP}\frac{dC_{SP}}{dt} = Q_{SP}\left(C_P - \frac{C_{SP}}{K_{p,SP}}\right)$$

(11) Thymus

$$V_{TH}\frac{dC_{TH}}{dt} = Q_{TH}\left(C_P - \frac{C_{TH}}{K_{p,TH}}\right)$$

(12) Rest of body

$$V_{RE}\frac{dC_{RE}}{dt} = Q_{RE}\left(C_P - \frac{C_{RE}}{K_{p,RE}}\right)$$

(13) Red blood cell

Unbound

$$\frac{dC_{RBC,U}}{dt} = \frac{V\text{maxfuC}_\text{P}}{Km+fuC_P} - \frac{PSBCC_{RBC,U}}{V_{RBC}} - konC_{RBC,U} + koffC_{RBC,B}$$

Bound

$$\frac{dC_{RBC,B}}{dt} = konC_{RBC,U} - koffC_{RBC,B}$$

References

1. Ramsey LB, Bruun GH, Yang W, Trevino LR, Vattathil S, Scheet P, Cheng C, Rosner GL, Giacomini KM, Fan Y, Sparreboom A, Mikkelsen TS, Corydon TJ, Pui CH, Evans WE, Relling MV (2012) Rare versus common variants in pharmacogenetics: SLCO1B1 variation and methotrexate disposition. Genome Res 22:1–8
2. Balis FM, Savitch JL, Bleyer WA (1983) Pharmacokinetics of oral methotrexate in children. Cancer Res 43:2342–2345
3. Edelman J, Biggs DF, Jamali F, Russell AS (1984) Low-dose methotrexate kinetics in arthritis. Clin Pharmacol Ther 35:382–386
4. Bannwarth B, Pehourcq F, Schaeverbeke T, Dehais J (1996) Clinical pharmacokinetics of low-dose pulse methotrexate in rheumatoid arthritis. Clin Pharmacokinet 30:194–210
5. Herman RA, Veng-Pedersen P, Hoffman J, Koehnke R, Furst DE (1989) Pharmacokinetics of low-dose methotrexate in rheumatoid arthritis patients. J Pharm Sci 78:165–171
6. Seideman P, Beck O, Eksborg S, Wennberg M (1993) The pharmacokinetics of methotrexate and its 7-hydroxy metabolite in patients with rheumatoid arthritis. Br J Clin Pharmacol 35:409–412
7. Breithaupt H, Kuenzlen E (1982) Pharmacokinetics of methotrexate and 7-hydroxymethotrexate following infusions of high-dose methotrexate. Cancer Treat Rep 66:1733–1741
8. Teresi ME, Crom WR, Choi KE, Mirro J, Evans WE (1987) Methotrexate bioavailability after oral and intramuscular administration in children. J Pediatr 110:788–792
9. Angelis-Stoforidis P, Vajda FJ, Christophidis N (1999) Methotrexate polyglutamate levels in circulating erythrocytes and polymorphs correlate with clinical efficacy in rheumatoid arthritis. Clin Exp Rheumatol 17:313–320
10. Dervieux T, Furst D, Lein DO, Capps R, Smith K, Caldwell J, Kremer J (2005) Pharmacogenetic and metabolite measurements are associated with clinical status in patients with rheumatoid arthritis treated with methotrexate: results of a multicentred cross sectional observational study. Ann Rheum Dis 64:1180–1185
11. Dervieux T, Furst D, Lein DO, Capps R, Smith K, Walsh M, Kremer J (2004) Polyglutamation of methotrexate with common polymorphisms in reduced folate carrier, aminoimidazole carboxamide ribonucleotide transformylase, and thymidylate synthase are associated with methotrexate effects in rheumatoid arthritis. Arthritis Rheum 50:2766–2774
12. Korell J, Stamp LK, Barclay ML, Dalrymple JM, Drake J, Zhang M, Duffull SB (2013) A population pharmacokinetic model for low-dose methotrexate and its polyglutamated metabolites in red blood cells. Clin Pharmacokinet 52:475–485
13. Csordas K, Hegyi M, Eipel OT, Muller J, Erdelyi DJ, Kovacs GT (2013) Comparison of pharmacokinetics and toxicity after high-dose methotrexate treatments in children with acute lymphoblastic leukemia. Anticancer Drugs 24:189–197
14. Matthews I, Kirkpatrick C, Holford N (2004) Quantitative justification for target concentration intervention—parameter variability and predictive performance using population pharmacokinetic models for aminoglycosides. Br J Clin Pharmacol 58:8–19
15. Joerger M, Ferreri AJM, Krahenbuhl S, Schellens JHM, Cerny T, Zucca E, Huitema ADR (2012) Dosing algorithm to target a predefined AUC in patients with primary central nervous system lymphoma receiving high dose methotrexate. Br J Clin Pharmacol 73:240–247
16. Joerger M, Huitema ADR, van den Bongard HJGD, Baas P, Schornagel JH, Schellens JHM, Beijnen JH (2006) Determinants of the elimination of methotrexate and 7-hydroxy-methotrexate following high-dose infusional therapy to cancer patients. Br J Clin Pharmacol 62:71–80
17. Joerger M, Huitema ADR, Krahenbuhl S, Schellens JHM, Cerny T, Reni M, Zucca E, Cavalli F, Ferreri AJM (2010) Methotrexate area under the curve is an important outcome predictor in patients with primary CNS lymphoma: a pharmacokinetic-pharmacodynamic analysis from the IELSG no. 20 trial. Br J Cancer 102:673–677
18. Johansson AM, Hill N, Perisoglou M, Whelan J, Karlsson MO, Standing JF (2011) A population pharmacokinetic/pharmacodynamic model of methotrexate and mucositis scores in osteosarcoma. Ther Drug Monit 33:711–718
19. Colom H, Farre R, Soy D, Peraire C, Cendros JM, Pardo N, Torrent M, Domenech J, Mangues MA (2009) Population pharmacokinetics of high-dose methotrexate after intravenous administration in pediatric patients with osteosarcoma. Ther Drug Monit 31:76–85
20. Godfrey C, Sweeney K, Miller K, Hamilton R, Kremer J (1998) The population pharmacokinetics of long-term methotrexate in rheumatoid arthritis. Br J Clin Pharmacol 46:369–376
21. Bischoff KB, Dedrick RL, Zaharko DS (1970) Preliminary model for methotrexate pharmacokinetics. J Pharm Sci 59:149–154
22. Bischoff KB, Dedrick RL, Zaharko DS, Longstreth JA (1971) Methotrexate pharmacokinetics. J Pharm Sci 60:1128–1133
23. Evans WE, Tsiatis A, Crom WR, Brodeur GM, Coburn TC, Pratt CB (1981) Pharmacokinetics of sustained serum methotrexate concentrations secondary to gastrointestinal obstruction. J Pharm Sci 70:1194–1198
24. Dedrick RL, Myers CE, Bungay PM, DeVita VT Jr (1978) Pharmacokinetic rationale for peritoneal drug administration in the treatment of ovarian cancer. Cancer Treat Rep 62:1–11
25. Scheufler E, Zetler G, Iven H (1981) Pharmacokinetics and organ distribution of methotrexate in the rat. Pharmacology 23:75–81
26. Lutz RJ, Dedrick RL, Straw JA, Hart MM, Klubes P, Zaharko DS (1975) The kinetics of methotrexate distribution in spontaneous canine lymphosarcoma. J Pharmacokinet Biopharm 3:77–97
27. Li J, Gwilt P (2002) The effect of malignant effusions on methotrexate disposition. Cancer Chemother Pharmacol 50: 373–382
28. Edginton AN, Schmitt W, Willmann S (2006) Development and evaluation of a generic physiologically based pharmacokinetic model for children. Clin Pharmacokinet 45:1013–1034
29. Gertz M, Houston JB, Galetin A (2011) Physiologically based pharmacokinetic modeling of intestinal first-pass metabolism of CYP3A substrates with high intestinal extraction. Drug Metab Dispos 39:1633–1642
30. Dedrick RL, Zaharko DS, Lutz RJ (1973) Transport and binding of methotrexate in vivo. J Pharm Sci 62:882–890
31. Dalrymple JM, Stamp LK, O'Donnell JL, Chapman PT, Zhang M, Barclay ML (2008) Pharmacokinetics of oral methotrexate in patients with rheumatoid arthritis. Arthritis Rheum 58:3299–3308
32. Stewart CF, Fleming RA, Arkin CR, Evans WE (1990) Coadministration of naproxen and low-dose methotrexate in patients with rheumatoid arthritis. Clin Pharmacol Ther 47:540–546
33. Nuernberg B, Koehnke R, Solsky M, Hoffman J, Furst DE (1990) Biliary elimination of low-dose methotrexate in humans. Arthritis Rheum 33:898–902
34. Valentin J (2002) Basic anatomical and physiological data for use in radiological protection: reference values: ICRP publication 89. Ann ICRP 32:1–277

35. Jamei M, Turner D, Yang J, Neuhoff S, Polak S, Rostami-Hodjegan A, Tucker G (2009) Population-based mechanistic prediction of oral drug absorption. AAPS J 11:225–237
36. Schornagel JH, Van Engelen ME, De Vos D (1982) Bioavailability of methotrexate tablets. Pharm Weekbl Sci 4:89–90
37. Stewart AL, Margison JM, Wilkinson PM, Lucas SB (1985) The pharmacokinetics of 7-hydroxymethotrexate following medium-dose methotrexate therapy. Cancer Chemother Pharmacol 14:165–167
38. Landaw EM, DiStefano JJ 3rd (1984) Multiexponential, multicompartmental, and noncompartmental modeling. II. Data analysis and statistical considerations. Am J Physiol 246:R665–R677
39. Johnson TN, Rostami-Hodjegan A, Tucker GT (2006) Prediction of the clearance of eleven drugs and associated variability in neonates, infants and children. Clin Pharmacokinet 45:931–956
40. Haycock GB, Schwartz GJ, Wisotsky DH (1978) Geometric method for measuring body surface area: a height-weight formula validated in infants, children, and adults. J Pediatr 93:62–66
41. DuBois D, DuBois EF (1916) A formula to estimate the approximate surface area if height and weight be known. Arch Intern Med 17:863–871
42. Yip R, Johnson C, Dallman PR (1984) Age-related changes in laboratory values used in the diagnosis of anemia and iron deficiency. Am J Clin Nutr 39:427–436
43. McNamara PJ, Alcorn J (2002) Protein binding predictions in infants. AAPS Pharm Sci 4:E4
44. West GB, Brown JH, Enquist BJ (1999) The fourth dimension of life: fractal geometry and allometric scaling of organisms. Science 284:1677–1679
45. GetData Graph Digitizer (2013) http://getdata-graph-digitizer.com/
46. Pouliquen A-L, Escalup L, Jourdan N, Cottu P, Faure P, Madelaine-Chambrin I (2011) Dose standardisation of anticancer drugs. Int J Clin Pharm 33:221–228
47. MATLAB 7.14.0.739. Natick, Massachusetts: The Math Works Inc.; R2012a
48. Hubner G, Sander O, Degner FL, Turck D, Rau R (1997) Lack of pharmacokinetic interaction of meloxicam with methotrexate in patients with rheumatoid arthritis. J Rheumatol 24: 845–851
49. Oguey D, Kolliker F, Gerber NJ, Reichen J (1992) Effect of food on the bioavailability of low-dose methotrexate in patients with rheumatoid arthritis. Arthritis Rheum 35:611–614
50. Pinkerton CR, Welshman SG, Kelly JG, Shanks RG, Bridges JM (1982) Pharmacokinetics of low-dose methotrexate in children receiving maintenance therapy for acute lymphoblastic leukaemia. Cancer Chemother Pharmacol 10:36–39
51. Wang YM, Sutow WW, Romsdahl MM, Perez C (1979) Age-related pharmacokinetics of high-dose methotrexate in patients with osteosarcoma. Cancer Treat Rep 63:405–410
52. Balis FM, Holcenberg JS, Poplack DG, Ge J, Sather HN, Murphy RF, Ames MM, Waskerwitz MJ, Tubergen DG, Zimm S, Gilchrist GS, Bleyer WA (1998) Pharmacokinetics and pharmacodynamics of oral methotrexate and mercaptopurine in children with lower risk acute lymphoblastic leukemia: a joint children's cancer group and pediatric oncology branch study. Blood 92:3569–3577
53. Pinkerton CR, Welshman SG, Dempsey SI, Bridges JM, Glasgow JF (1980) Absorption of methotrexate under standardized conditions in children with acute lymphoblastic leukaemia. Br J Cancer 42:613–615
54. Maharaj AR, Barrett JS, Edginton AN (2013) A workflow example of PBPK modeling to support pediatric research and development: case study with lorazepam. AAPS J 15:455–464
55. International Transporter C, Giacomini KM, Huang SM, Tweedie DJ, Benet LZ, Brouwer KL, Chu X, Dahlin A, Evers R, Fischer V, Hillgren KM, Hoffmaster KA, Ishikawa T, Keppler D, Kim RB, Lee CA, Niemi M, Polli JW, Sugiyama Y, Swaan PW, Ware JA, Wright SH, Yee SW, Zamek-Gliszczynski MJ, Zhang L (2010) Membrane transporters in drug development. Nat Rev Drug Discov 9:215–236
56. Ramsey LB, Panetta JC, Smith C, Yang W, Fan Y, Winick NJ, Martin PL, Cheng C, Devidas M, Pui CH, Evans WE, Hunger SP, Loh M, Relling MV (2013) Genome-wide study of methotrexate clearance replicates SLCO1B1. Blood 121:898–904
57. Vlaming ML, Pala Z, van Esch A, Wagenaar E, van Tellingen O, de Waart DR, Oude Elferink RP, van de Wetering K, Schinkel AH (2008) Impact of Abcc2 (Mrp2) and Abcc3 (Mrp3) on the in vivo elimination of methotrexate and its main toxic metabolite 7-hydroxymethotrexate. Clin Cancer Res 14:8152–8160
58. Symcyp (2008) Simcyp Limited, Sheffield
59. Hall JE (2011) Guyton and hall textbook of medical physiology/ John E. Hall. Philadelphia, PA : Saunders Elsevier, Philadelphia, PA
60. Stewart CF, Fleming RA, Germain BF, Seleznick MJ, Evans WE (1991) Aspirin alters methotrexate disposition in rheumatoid arthritis patients. Arthritis Rheum 34:1514–1520
61. Hroch M, Chladek J, Simkova M, Vaneckova J, Grim J, Martinkova J (2008) A pilot study of pharmacokinetically guided dosing of oral methotrexate in the initial phase of psoriasis treatment. J Eur Acad Dermatol Venereol 22:19–24
62. Kozloski GD, De Vito JM, Kisicki JC, Johnson JB (1992) The effect of food on the absorption of methotrexate sodium tablets in healthy volunteers. Arthritis Rheum 35:761–764